How light absorbing properties of organic aerosol modify the Asian summer monsoon rainfall?

Jung-Eun Chu[1,2], Kyu-Myong Kim[3], William K. M. Lau[4] and Kyung-Ja Ha[1,2]*

[1]Center for Climate Physics, Institute for Basic Science (IBS), Busan, South Korea, 46241.
[2]Department of Atmospheric Sciences, Pusan National University, Busan, South Korea, 46241.
[3]Climate and Radiation Laboratory, NASA Goddard Space Flight Center, Greenbelt, MD, United States, 20771.
[4]Earth System Science Interdisciplinary Center, University of Maryland, College Park, MD, United States, 20740.

Corresponding Author: Prof. Kyung-Ja Ha (kjha@pusan.ac.kr)
†Address: Center for Climate Physics, Institute for Basic Science (IBS), Busan, South Korea, 46241 and Department of Atmospheric Sciences, Pusan National University, Busan, South Korea, 46241
Phone: +82-51-510-7860; Fax: +82-51-510-7694; E-mail: kjha@pusan.ac.kr

Key Points:

- Impact of enhanced OA light absorption on Asian summer monsoon is examined using observations and an AGCM experiment
- OA light absorption acts to advance the Indian summer monsoon and shift East Asian summer monsoon rain band southward
- The effects of OA light absorption in aerosol-monsoon interaction can be substantial and cannot be ignored

Abstract

Light absorbing aerosols not only contribute to Earth's radiative balance but also influence regional climate by cooling the surface and warming the atmosphere. Following recent suggestions that organic aerosols (OAs) absorb substantial amount of solar radiation, we examine the role of light absorbing properties of OA on Asian summer monsoon rainfall redistribution using observational data and an atmospheric general circulation model (AGCM) experiment. Results suggest that the enhanced light absorption by OA in Southeast Asia and Northeast Asia are associated with the advance of the Indian summer monsoon in May and the southward shift of East Asian summer monsoon rain band in June. The rainfall redistribution in May is induced by elevated orographic effect with a warm-core upper-level anticyclone and surface warming of 1-2^{o}C over the Tibetan Plateau whereas that of the East Asian summer monsoon in June is formed by stable conditions associated with surface cooling and atmospheric warming around 30°N.

1. Introduction

Asia accounts for nearly 30% of the global anthropogenic organic carbon emissions, which are mostly due to fossil- and biofuel usage (Bond et al., 2004). In this region, about 2500 Gg/yr of organic carbons from open biomass burning are emitted, mostly from Southeast Asia (Bond et al., 2004). Asia is the region most vulnerable to natural hazards because of the summer monsoon and a large population accounting for nearly 60% of the global population. During the last decade, it has been reported that organic aerosols (OAs) absorb substantial amounts of sunlight (Andreae & Gelencsér, 2006; Alexander et al., 2008; Chen & Bond, 2010; Bahadur et al., 2012; Chu & Ha, 2016). However, most climate models have treated OAs as scattering or weakly absorbing species (e.g., Takemura et al., 2005, 2009; Myhre et al., 2007; Myhre, 2009; Zhang et al., 2009). The light absorption by particles, which have wavelength much smaller than the wavelength of incident light, is proportional to the mass and volume (Moosmüller et al., 2009); the underestimation of OA light absorption in climate models may lead to a large bias in climatic response estimates.

The light absorbing OA is also called as “brown carbon” due to its strong absorption toward shorter wavelength (Andreae & Gelencsér, 2006). After scientists started to distinguish OA (or brown carbon) from black carbon (BC) in early 2000s, there has been substantial progresses in understanding of chemical and optical properties of brown carbon (a review paper by Laskin et al. 2015), aging processes (Huang et al. 2013), and radiative forcing (Chung et al, 2012; Feng et al. 2013). One of the most striking results for climate science was that the contribution of brown carbon on light absorption at 550 nm corresponds to 20% of total carbonaceous aerosol absorption (Chung et al. 2012) and as large as 56% at 380 nm (Feng et al. 2013). However, mixing state of light absorbing organic carbon to purely scattering organic carbon in the atmosphere is still remains unknown. For this reason, we will

refer to atmospheric column averaged particulate state of the mixture of light absorbing and scattering organic carbon as OA.

Despite of the importance of light absorption by OA, previous studies on the climatic effect of light absorbing aerosol have considered BC as the only absorber (Menon et al., 2002; Wang, 2007; Ramanathan & Carmichael, 2008). For example, Menon et al. (2002) considered BC to be the sole absorber and implemented two experiments by including aerosols with a single scattering albedo (SSA) of 0.85 and 1.0, respectively, representative of the appropriate amount of BC; the remainder is sulfate aerosol. There are some other studies who considered additional absorption by dust aerosols (Lau et al., 2006; 2010). Lau et al. (2006) treated BC and dust as absorbing aerosols and showed that the increased dust load together with BC emission from local sources in northern India during late spring may lead to an advance of the rainy period and subsequently intensify the early stage of the Indian summer monsoon. Few studies have implemented climate model simulations with OA light absorption. Park et al. (2010) have shown that the inclusion of light absorbing OAs in climate models results in a better agreement with the observed aerosol light absorption in East Asia. However, they focused on radiative effect of OA on Asian climate. It remains questionable whether more realistic treatment of OA light absorption would cause significant changes in circulation and precipitation in Asian monsoon region. If so, what is the detailed response and magnitude of the monsoon system in response to the changes in OA light absorption?

This study aims to determine the impact of enhanced light absorption by OAs on the Asian monsoon climate. Recently, Chu & Ha (2016) developed an observationally constrained algorithm to quantify the OA light absorption using ground-based Aerosol Robotic Network (AERONET) observations and obtained a OA SSA value of 0.91 (0.82–0.93). Following recent suggestions that OAs absorb substantial amount of solar radiation, we conducted two primary experiments, EXP_ABS and EXP_SCA, with OA SSAs of 0.91 and

1.0, indicating light absorbing OAs and purely scattering OAs, respectively. Data and experiment design are described in section 2. In section 3, we discuss the observed impact of biomass burning on the Asian monsoon climate and explore the mechanisms by which OA light absorption influence the Asian summer monsoon using differences between EXP_ABS and EXP_SCA experiments. Section 4 is for summary and discussions.

2. Data and Experimental design

2.1 Data

The Fire Energetics and Emissions Research (FEER) is a satellite-based top-down emission estimates developed by NASA (Ichoku & Ellison, 2014). We downloaded FEER v.1 emission estimates of total carbon (TC) based on MODIS 2003–2013 Fire Radiative Power and aerosol optical thickness observations from the Moderate-resolution Imaging Spectro-radiometer (MODIS) sensors aboard the Terra and Aqua on a 0.5° x 0.5°-resolution global grid (http://feer.gsfc.nasa.gov). Surface temperature, zonal and meridional winds at 850 hPa are obtained from the National Centers for Environmental Prediction-National Center for Atmospheric Research (NCEP-NCAR) reanalysis product with 2.5° x 2.5°-resolution (Kalnay et al. 1996). The precipitation data are obtained from Global Precipitation Climatology Project (GPCP).

2.2 Experimental design

We performed numerical experiments with the Community Atmosphere Model version 4 (CAM4), which is the seventh generation of atmospheric general circulation model (AGCM) developed by NCAR (Neale et al., 2013). The horizontal resolution of the model is T42, which has approximately 2.8 × 2.8 degrees with the finite volume dynamical core. There are

26 vertical layers (with a top at 3 hPa). During the initialization process, the three-dimensional time-dependent monthly mean distribution of the eleven aerosol masses and the optics for each species are prescribed into CAM4. The eleven aerosol species include natural and anthropogenic sulfate, two size bins of sea-salt, four-size bins of soil dust with diameters from 0.1 to 10 μm, new and aged BCs, and hydrophobic and hydrophilic OAs. The sulfate, sea-salt, and hydrophilic organic carbon are affected by hygroscopic growth. The default aerosol climatology prescribed in CAM4 is produced using the Model for Atmospheric Chemistry and Transport (MATCH) (Rasch et al., 1997) integrated using the National Centers for Environmental Prediction (NCEP) meteorological reanalysis and an assimilation of satellite retrievals of aerosol optical depth (AOD) from the NOAA Pathfinder II data set (Stowe et al., 1997). The emissions of carbonaceous aerosols include contributions from biomass burning, fossil fuel burning, and a source of natural organic aerosols resulting from terpene emissions. The injection height for savanna, forest, and open-fires are the first 2000m whereas that for fossil fuel is the boundary layer (Liousse et al., 1996). The optical properties for BC are same as in the optics for soot and water-soluble aerosols in the Optical Properties of Aerosols and Clouds (OPAC) dataset (Hess et al., 1998). The SOA is not considered in this version. Regarding aerosol optical properties, the specific extinction, SSA, and asymmetry parameter are prescribed as globally uniform and time-independent constants for each of the eleven aerosols. Dust aerosol is from Mie calculations for the size distribution represented by each size bin (Zender et al., 2003). The sulfate aerosol is assumed to be composed of ammonium sulfate with a long-normal size distribution and the nitrate aerosol is not included. The optical properties of the individual aerosol species are combined by the bulk formulae of Cess (1985) to represent the aerosol optical properties for each layer. The cloud formation scheme in CAM4 follows the same deep parameterization of Zhang-McFarlane approach same as in CAM3 (Collins et al. 2006), where shallow convection

follows Hack et al. (2006). Detailed information on the clouds and precipitation process can be found in Boville et al. (2006).

To isolate the impact of OA light absorption, we fixed the amounts of greenhouse gases and prescribed aerosols. The model is forced with the observed climatological SST and sea ice distribution. The control experiment has been conducted for ten years, with four ensemble members based on the year 2000 condition; the first five years of the ten-year experiments are removed and the last five years of each experiment (i.e., 5 years × 4 ensemble members) were used for our analysis. To investigate the impact of OA light absorption on the Asian monsoon climate, we conducted two primary experiments, EXP_ABS and EXP_SCA, with OA SSAs of 0.91 and 1.0, indicating light absorbing OAs and purely scattering OAs, respectively. Each set of the experiment has four ensemble members. The OA SSA value of 0.91 was obtained from the study by Chu & Ha (2016) in which the OA SSA was empirically determined using ground-based observations. Because CAM4 uses prescribed bulk aerosol, the difference between EXP_ABS and EXP_SCA represents the climate response solely due to enhanced OA light absorption.

It should be noted that there are large discrepancies in AOD and fine-mode AOD (fAOD) distribution between observation and CAM4 simulation. Generally, AOD in CAM4 is underestimated over most regions and the difference is as large as 5 times in the major hotspots including Asia and Indo-Gangetic Plains. The global mean AOD and fAOD in CAM4 default simulation are underestimated by 40% and 20%, respectively. For this reason, we conducted a control experiment prescribed with aerosol mass concentration constrained by observations. To constrain aerosol concentrations, we integrated the model for 20 years with CAM4 default aerosol emission data. Then, we calculated ratio of observed AOD to simulated AOD for each grid cell over the whole globe. The control experiment is a simulation with aerosol concentrations multiplied with the ratio to infer more realistic aerosol

167 distribution. The observed AOD is obtained from Chung et al. (2012) and Lee & Chung
168 (2013) who estimated AOD and fAOD globally by integrating monthly satellite-based
169 (MODIS and MISR) and ground-based AERONET observations based on 2001 to 2010
170 period. The aerosol concentration is constrained at first for fine-mode aerosols (diameter less
171 than 2.5 μm) to fit with observed fAOD, and rest of aerosol species are multiplied by ratio of
172 observed AOD minus fAOD to simulated AOD minus fAOD. By using this observationally
173 constrained AOD method, spacial distribution of AOD and fAOD are substantially improved
174 especially over Asia and Indo-Gangetic Plains. The improvements of AOD and fAOD
175 averaged over Asian region in the control experiment (i.e., observationally constrained
176 experiment) relative to the CAM4 default simulation corresponds to 38% and 100%,
177 respectively. The underestimated AOD in model is likely caused by an underestimation of
178 dust aerosols and overestimation of its wet and dry deposition processes. Our analysis,
179 however, multiplied fine-mode aerosols including BC, OA, sulfate, one out of the four dust
180 aerosols, and one out of the two sea-salt aerosols by the same observation-to-model ratio. The
181 uncertainty in our experiment can be caused by the ratio which is overwhelmed by sulfate
182 aerosol, the most dominant species in Asian region. The uncertainty in observed dataset are
183 discussed in Chung et al. (2012) and Lee & Chung (2013).
184
185 **3. Results**
186 **3.1 Observed absorbing aerosol and Asian monsoon interaction**
187 In the pre-monsoon period in March/April, extremely large amounts of organic particles
188 are emitted to the atmosphere due to open agricultural biomass burning in Southeast Asia
189 (Figure 1). Despite of the high altitudes, these organic particles sometimes penetrate the
190 southern slope of the Himalayas (Bonasoni et al., 2010; Cong et al., 2015). Together with

local sources, the transported aerosols cause hazardous haze pollution in India and Southeast Asia every year. We first examined if there is any regional consensus in the climate response in high-emission years in the major biomass-burning region. Based on top-down estimation of TC emission during 2003-2013 period, we calculated the composite difference between high- and low-emission years. The high- and low-emission years were selected based on the accumulated FEER TC emission product of the mainland of Southeast Asia (15°N–25°N, 90°E–105°E) from March to April. The selected high-emission years include 2004, 2007, 2010, and 2012; low-emissions years include 2003, 2005, 2008, and 2011. It should be noted that the year 2013 was omitted from the low-emission years because the 2013 value is not notably different from that observed in the previous year and the emission in March, the most abundant month, does not display lower levels than other low-emission years.

Figure 2 shows the composite differences in surface temperature, precipitation, and low-level streamlines at 850 hPa between high- and low-emission years from March to June. The high emission of TC over Southeast Asia is accompanied by an anomalously high surface temperature and dry conditions in the inland area of Southeast Asia in March, where biomass is burned almost every year. This warm and dry anomaly in March can be interpreted as pre-condition, which is favorable for active biomass burning, rather than the response of OA light absorption. In April, however, the surface temperature shows a decrease in Southeast Asia and a significant increase for the entire Indian subcontinent (Figure 2a). Significant positive precipitation anomalies were found over the northern inland part of the Bay of Bengal and Southeast China (Figure 2b). From May to June, the surface temperature seems to increase over the southern slopes of the Tibetan Plateau; however, not statistically significant. On the other hand, the circulation and precipitation patterns display the significantly intensified southwesterly monsoon over the coastal Arabian Sea in May and the weakened anticyclonic circulation (i.e., anomalous cyclonic circulation) over both Indian and East Asian monsoon

regions in June. However, the biomass burning events and changes in precipitation in Southeast Asia, have often been associated with large-scale SST forcing, such as the El Niño-Southern Oscillation (Inness et al. 2015). Yet, the sole effect of OA light absorption on the Asian monsoon system is unknown. Therefore, it is necessary to examine the response of the Asian monsoon to OA light absorption using a fixed SST experiment.

3.2 Simulated impact of OA light absorption

Figure 3 shows the vertically integrated organic carbon concentration prescribed in CAM4 and simulated changes in surface temperature, precipitation, and low-level circulation from April to June. We found an excellent correspondence of the surface temperature and precipitation between observation and simulation. In April, the OA light absorption leads to a cool temperature anomaly over Southeast Asia around the source region and a warm anomaly over the western part covering the Indian subcontinent and western Eurasia. The pronounced surface temperature cooling is related to the increased rainfall over Southeast Asia around the source region (Figure 3b). In May, the temperature anomaly field shows a positive change over the southern part of the Tibetan Plateau and an upper level high over the region of warming. A striking increase of precipitation was observed over the Indian subcontinent, which is related to the enhanced southwesterly monsoon flow transporting more moisture to the Indian subcontinent (Figure 3c). In June, the largest surface temperature warming was detected over the Himalayas and Tibetan Plateau, whereas the surface cooling over western Eurasia contrasts the observation. An increased rainfall pattern was observed over the northern Arabian Sea, eastern Himalayas, and East Asia stretching from the South China Sea to southern Japan, whereas decreased rainfall was reported for the entire Indian subcontinent, Tibetan Plateau, and East Asia including the Yangtze River, Korea, and Japan. The

suppressed Indian summer monsoon precipitation and southward displacement of the East Asian summer monsoon rain belt, which is called Meiyu–Changma–Baiu, with cyclonic circulation, represent the weakening of the Indian and East Asian summer monsoon rainfall. The overall results that showing the advance of Indian summer monsoon and weakening of East Asian summer monsoon rainfall from model simulations suggest that the enhanced light absorption by OAs can lead to a change of the Asian summer monsoon rainfall and circulation, which is generally similar to the observed pattern. However, what is the OA light absorption mechanism leading to the advance of the Indian summer monsoon and weakening of East Asia summer monsoon rainfall? This question will be addressed in the remainder of this paper.

3.3 Mechanisms by which OA light absorption influences the Asian summer monsoon

Figure 4 to Figure 7 show month-to-month atmospheric responses due to OA light absorption to determine the mechanisms that drive significant changes of the Asian monsoon climate. The atmospheric responses are represented by the latitude- or longitude–height cross sections of air temperature (K), vertical circulation (m/s), specific humidity (g/kg), and solar heating rates (K/day) for each month. Because the longwave heating is relatively small, the shortwave heating represents the fundamental aerosol and cloud forcing that triggers the response of atmospheric circulation.

In April, the OA forcing is located at the southern and southeastern slopes of the Himalayas at approximately 90°E–110°E (Figure 3a). The warm southeastern slope directly derives low-level convergence and consequent upward motion due to the elevated orographic effect (Figure 4a). The convergence and upward motion cause the increase in precipitation at 90°E–100°E, which leads to the decrease of the surface temperature (Figure 4b). The strong

positive solar heating rate over the upper level (300–400 hPa) on the eastern side of Tibetan Plateau (100°E–130°E) as shown in Figure 4a is due to the increased middle to high clouds as a response of positive low-level solar heating rate (i.e., aerosol semi-direct effect). The surface to upper tropospheric cooling over the region along 100°E–130°E is due to the cloud dimming effect rather than the direct effect by OA absorption, because the surface cooling stabilizes the atmospheric column, which cannot explain the local precipitation anomaly. Moving downslope from a mountain range, the western side of the Himalayas experiences significantly warm and dry conditions due to adiabatic heating (Figure 4b). The surface energy budget and contribution of the sensible heat flux is presented in Table 1. The surface energy balance over the Indian continent is largely affected by sensible heat flux in April. Since flux value is positive upward, strong negative sensible heat flux indicates that energy is transferred downward from atmosphere to surface.

One may argue that an initial increase in westerly flow over Indian continent in April will bring in more dust from the Middle East desert across the Arabian Sea and light absorption by dust aerosol can also contribute to the anomalies. However, we couldn't find any significant increase in dust AOD over the Arabian Sea and Indian continent, even though previous studies have shown that rainfall over the northeast India has been sensitive to dust aerosol over Arabian Sea via remote forcing (Vinoj et al., 2014; Lau et al., 2017). Therefore, the OA-derived adiabatic heating may be the reason we can see the surface temperature warming over India. On the other hand, pronounced positive surface temperature anomalies are seen over a wide area of Eurasia, especially over the area from India to Kazakhstan covering the west of Tibetan Plateau. The west of Tibetan Plateau, especially the conjunction areas between the Karakoram and Kunlun glacier mountains exhibit more than 70% of snow/ice covered days annually (Qian et al. 2011). The pronounced surface warming over the western Tibetan Plateau and adjacent region is directly linked to the accelerated snow melt

290 over that region (Figure 5). The OA-induced surface warming melts snow, lowering the
291 surface albedo, which in turn leads to more solar energy absorption, warming the surface
292 further. Figure 5 shows the increased net surface shortwave radiation over the snow surface
293 of Tibetan Plateau due to snow albedo effect (snow darkening effect). It may be the reason,
294 why even the perturbation forcing is applied only over Southeast Asia, the response is near
295 global. However, since CAM model tends to over-predict snow cover fraction compared to
296 satellite observations from November to April (Qian et al. 2011), care should be taken not to
297 overestimate the warming effect of snow melting.

298 The onset of the Asian summer monsoon is accompanied by a seasonal reversal of the
299 prevailing wind direction and moisture advection by wind (Liu et al., 2015). The wind
300 reversal is associated with the warmer Indian continent than adjacent ocean due to the
301 different response of land and ocean to solar heating. The results shown in Figure 6a
302 demonstrate that the OA light absorption effect causes stronger southwesterly flow in May
303 due to the relatively warm conditions of the Indian continent, which enhances the meridional
304 temperature gradient and accelerates moisture transport from the Arabian Sea to the Indian
305 subcontinent (Roxy et al., 2015). The near surface air over northern India and the southern
306 slope of the Tibetan Plateau therefore becomes warmer and wetter (Figure 6b). At the same
307 time, the ascent air around the north (15°N–25°N) and descent air around the south (EQ–10°N)
308 intensify the monsoonal meridional circulation, featuring a thermally direct circulation with
309 low-level warm moist air rising and cold air sinking (Figure 6a). The changes of the
310 atmospheric and surface conditions in the Indian monsoon region during the pre-monsoon
311 period (April to May) act to advance the Indian summer monsoon to May. It is interesting to
312 note that the advanced and intensified Indian monsoon in response to OA light absorption
313 displays patterns similar to the "elevated heat pump (EHP)" effect (Lau et al., 2006; Lau &
314 Kim, 2006). Through model experiments and observations, Lau et al. (2006) and Lau and

315 Kim (2006) suggested that dust aerosols reinforced by the heavy load of BC from industrial
316 pollution over the Indo–Gangetic Basin during the pre-monsoon period induce the rising
317 motion over the southern slope of the Tibetan Plateau and draw warm and moist low-level in
318 the Indian continent. However, the previous EHP theory focused on light absorption by
319 transported dust and local BC aerosols over the slope of an elevated region. Here we
320 demonstrate that regardless of the presence of BC and dust, the OA light absorption acts to
321 advance the Indian summer monsoon rainfall, in a manner similar to the EHP effect through
322 dynamical adjustment to aerosol-induced heating gradient.

323 Meanwhile, the surface warming induced by the early melting of snow on the southern
324 slope of the Himalayas during April and May is further intensified due to increased incoming
325 shortwave radiation over the entire Tibetan Plateau in June (Table 1). This surface warming
326 is associated with formation of a warm-core upper-level anticyclone and surface warming of
327 1-2^{o}C over the Tibetan Plateau (bottom in Figure 3b). The surface warming and upward
328 motion in the southern slope of Tibetan Plateau are accompanied by a notable descent to its
329 south around 20°N, which in turn act to suppress rainfall over the entire Indian continent in
330 June (Figure 3c). At the same time, anomalous low-level cyclonic circulation can be observed
331 along a southwest–northeast-oriented rain belt extending from the South China Sea to
332 southern Japan. Climatologically, the East Asian rain band is located at ~30°N where
333 abundant OA exits in the lower level (Figure 3a) and it extends from the mid-lower reach of
334 the Yangtze River Valley across South Korea to eastern Japan. The anomalous rainfall
335 pattern with the southwest–northeast-oriented rain belt from the experiment is located further
336 south than the climatological East Asian subtropical front. The zonally elongated negative
337 rainfall anomaly north of the positive anomaly demonstrates that the East Asian subtropical
338 front is shifted southward. This is further supported by the vertical cross section of the solar
339 heating rate and latitudinal temperature profile (Figure 7). Compared to other regions, the OA

concentration in East Asia is located north of 30°N and peaks in low-level below 850 hPa (see bottom panel in Figure 3a). This is partly because the formation process of OA in East Asia is dominated by incomplete combustion of either fossil fuel or biofuel whereas that of Southeast Asia is dominated by biomass burning (Bond et al. 2004). Heald et al. (2011) examined the vertical profile of OA based on aircraft campaigns and noted that East Asian region has OA peak in boundary layer below 1.5 km whereas that of biomass burning has elevated layers aloft through the free troposphere. Surface cooling over north of 30°N by extinction of the light by OA increases the atmospheric stability, which in turn blocks the northward migration of the zonal rain band. The East Asian summer monsoon rain belt therefore shifts southward. The solar heating rate field in the Figure 7 is located in the same latitude with a strong upward motion and positive temperature anomaly near 20°N-25°N. In other words, the positive heating rate anomaly near 20°N-25°N is related to the water vapor heating by shifted convection, not due to OA concentration. On the other hand, cooling over the north of 30°N seems to secondary downward flow driven by northerly flow (~28°N) to compensate strong upward motion in the south. The dry adiabatic warming forced by secondary downward flow in north of 30°N may perturb the surface cooling in China (Figure 3b). In brief, initial surface radiative cooling over north of 30°N is responsible for southward shift of East Asian rain belt whereas secondary downward flow is responsible for more atmospheric cooling and less surface cooling over China.

4. Summary and Discussion

The OAs are considered to be the second most important contributors to atmospheric fine particles in Asia, except during the dust-dominated season. Especially, open agricultural biomass burning during the pre-monsoon period in Southeast Asia emits extremely large

364 amounts of organic particles every year. Although the light absorption by atmospheric OAs is
365 reported to be larger than currently believed, most of the climate models treat OAs as
366 scattering or weakly absorbing species. This study examines how light absorbing properties
367 of OA influence Asian summer monsoon rainfall redistribution and circulation change.
368 Observational evidences show that anomalous heating by absorbing aerosols can cause the
369 advance of the Indian monsoon rainy season in May and southward shift of East Asian
370 monsoon rain band in June. The AGCM experiment display similar results with observation.
371 Figure 8 summarizes the mechanisms of the effect of OA light absorption on Asian summer
372 monsoon. The initial OA forcing from biomass burning over the mainland of southeast Asia
373 (15°N–25°N, 90°E–105°E) derives convergence and upward wind due to the orographic effect
374 on the western boundaries in April. India experiences warm and dry condition due to
375 adiabatic of downward moving air. This warmer and drier pre-monsoon condition invigorates
376 Indian summer monsoon and strengthens monsoon meridional overturning circulation in May
377 (Figure 8b). In June, the warm-core high intensified over the entire Tibetan Plateau because
378 of early melting of snow and increased incoming shortwave radiation. It supports that the
379 mechanisms through which the atmosphere response to light absorbing properties of OA over
380 South Asia occur in a manner similar to the EHP effect over Indian summer monsoon region.
381 Although the EHP effect focused on different absorbing aerosol species from this study (i.e.,
382 BC and dust aerosols in EHP effect, and OAs in this study), our results imply that the
383 aerosol-induced rising air forced by the elevated region draws warm and moist air from
384 below accelerating the initial warming. On the other hand, aerosol-induced atmospheric
385 warming and surface cooling over the region without topographic effect (i.e., Northeast Asia)
386 acts to increase atmospheric stability inhibiting northward propagation of East Asian rain
387 band (Figure 8c). The results clearly show that regardless of the presence of BC and dust
388 aerosols, light absorption by OA can cause a significant large-scale dynamical adjustment to

aerosol-induced horizontal and vertical heating gradients of the atmosphere and land surface.

In addition to dynamical adjustment to aerosol-induced heating, aerosol and monsoon interact with each other (Lau et al. 2016). The model used in this study is not an interactive model and does not include changes in emission due to changes in meteorological fields. Recent studies by Lou et al. (2016; 2017) examined the impacts of changes in springtime and wintertime East Asian monsoon strengths on dust emissions in China by using interactive model experiment. They demonstrated that dust-wind speed feedback enhanced the impact of the East Asian Monsoon and net radiative forcing over eastern China by about 40%. Furthermore, Yang et al. (2017) further identified that decreases in wind speed derived reduction in dust emission over northern China during wintertime, resulting in enhanced stagnant and increased concentration of anthropogenic aerosol pollution over east China. Further study will be needed to examine the impact of monsoon on OA emission over the South and Southeast Asian region.

Although this study only considered the aerosol direct and semi-direct effects, the indirect effect of aerosol by modulating cloud microphysics can also influence rainfall redistribution during monsoon period. Recently, Lau et al. (2017) conducted numerical forecast experiments of aerosol radiative and aerosol-cloud-microphysics effects to investigate the aerosol-monsoon interaction over the northern Indian Himalaya foothill region. They suggested that aerosol radiative effect and dynamic feedback dominate the large-scale response, but microphysics effect can further enhance the aerosol radiative interaction in invigorating the deep cloud process and accelerating the transformation of the monsoon depression into intense meso-scale cells with heavy rain. Huang et al. (2013) also suggested that atmospheric aging process by converting from hydrophobic to hydrophilic OA played an important role in affecting the lifetime and atmospheric burden of OA, implying a possible impact on radiative forcing and cloud formation/lifetime. We expect that impact of abundant

biomass burning aerosols over Southeast Asia and its light absorbing properties will be large enough to change regional cloud microphysics during pre-monsoon period. Further study should be conducted to better understand microphysics effect of light absorbing OA. Given the evidences shown in this study, we would like to argue that pre-monsoon aerosol can play a substantial impact on evolution and intensity of monsoon. Hence, it may be possible to use pre-monsoon aerosol as a predictor of precipitation over the monsoon region.

Acknowledgements

This work was supported by IBS-R028-D1. This research was also supported by Global Research Laboratory (GRL) grant (MEST 2011-0021927) and the Fostering Core Leaders of the Future Basic Science Program (NRF-2013H1A8A1004201) funded by the National Research Foundation (NRF) of Korea. We thank two anonymous reviewers for their constructive comments. FEER total carbon data can be found at https://feer.gsfc.nasa.gov/data/emissions/, NCEP-NCAR reanalysis data at https://www.esrl.noaa.gov/psd/data/gridded/data.ncep.reanalysis.html, and GPCP precipitation data at https://www.esrl.noaa.gov/psd/data/gridded/data.gpcp.html. The CESM model used in this study can be downloaded from http://www.cesm.ucar.edu/models/cesm1.0.

Figure or Table Captions

Figure 1. Springtime biomass burning emission over Asian region. The biomass burning emission is obtained from Fire Energetics and Emissions Research (FEER) v.1 emission estimates of total carbon (TC) based on MODIS 2003–2013 Fire Radiative Power and AOT observations from Terra and Aqua. The emission data is averaged for March to April on a 0.5° x 0.5°-resolution global grid. The time series in the red box is March to April averaged TC emissions over Southeast Asia (15^{o}N-25^{o}N, 90^{o}E-105^{o}E).

Figure 2. Observed composite differences between strong and weak TC emission years. (a) Surface temperature and (b) precipitation and streamlines at 850 hPa from March to June. The strong and weak emission years were selected based on the accumulated TC emission from March to April over Southeast Asia (15°N–25°N, 90°E–105°E). The selected high- and low-emission years are 2004, 2007, 2010, and 2012 and 2003, 2005, 2008, and 2011, respectively. The crosshatched areas indicate a statistical significance of the Student's t-test at the 90% level.

Figure 3. Prescribed OA concentration and changes in Asian monsoon climate due to enhanced OA light absorption obtained from CAM4 experiments. The left panel (a) indicates the vertically integrated organic carbon concentration (10^{-6} g/kg) prescribed in CAM4, the middle panel (b) represents changes in surface temperature (shading) and geopotential height at 300 hPa, and right panel is for (c) precipitation (shading) and 850 hPa (vector) streamlines for April (upper), May (middle), and June (lower). The crosshatched areas indicate statistical significance of the Student's t-test at the 90% level. The organic carbon is the sum of the hydrophobic and hydrophilic organic carbon.

Figure 4. Longitude-height cross section of the atmospheric response to OA heating over southeast Asian region in April. (a) Solar heating rate (QRS, shading) and wind anomalies (vector) and (b) air temperature (T, shading) and specific humidity (SH, contour). The graphs are latitudinally averaged over 20°N–30°N to examine upward motion around the source region. The unit of the vertical velocity (specific humidity) is $2*10^{-2}$ ms^{-1} (0.05 g/kg). The positive (negative) values for SH are plotted as solid (dashed) lines.

Figure 5. Monthly snow fraction and net downward shortwave flux at surface associated with enhanced OA light absorption. The shading indicates mean snow fraction in EXP_SCA experiment and blue and orange contours represent changes in snow fraction and shortwave

463 flux (i.e., EXP_ABS minus EXP_SCA). The graphs are longitudinally averaged over 70°E-
464 90°E to examined OA impact on snow melting over Tibetan Plateau. The units of the fluxes
465 are Wm^{-2}. Contour interval for snow fraction is 0.01 and that for shortwave is 3 Wm^{-2}. The
466 positive (negative) values are plotted as solid (dashed) lines.

467 **Figure 6.** Latitude-height cross section averaged over 70°E–90°E in May. (a) QRS (shading)
468 and wind anomalies (vector) and (b) T (shading) and SH (contour). The graphs are
469 longitudinally averaged over 70°E–90°E to examine enhanced meridional overturning
470 circulation and strengthening of Indian summer monsoon.

471 **Figure 7.** Same as in Figure 6 but averaged over 110°E–130°E in June.

472 **Figure 8.** Schematic diagram of OA light absorption effect. Figure summarizes the
473 mechanisms of how the OA light absorption influences Asian summer monsoon from April
474 to June.

475 **Table 1.** Changes in surface energy balance over Indian continent and Tibetan Plateau.

476 **Table 1.** Changes in surface energy balance over Indian continent and Tibetan Plateau.

[Wm^{-2}]	**India**	**Tibetan Plateau**		
	April	**April**	**May**	**June**
Net downward shortwave flux (SW)	-5.74	21.09	8.73	47.28
Net upward longwave flux (LW)	-4.33	11.78	12.34	33.96
Upward sensible heat flux (SH)	-11.97	-0.81	9.21	27.71
Upward latent heat flux (LH)	9.81	5.09	-9.82	-16.43
Net surface energy balance	0.74	5.03	-3.00	2.05

477 *Note.* All fluxes except for shortwave flux are positive upward. Net surface energy balance is
478 defined as SW-LW-SH-LH. Area for Indian continent (20°N-30°N, 70°E-90°E) and Tibetan
479 Plateau (30°N-40°N, 80°E-100°E) correspond to yellow boxes in Figure 3b.
480
481

References

Alexander, D. T. L., Crozier, P. A., & Anderson, J. R. (2008). Brown Carbon Spheres in East Asian Outflow and Their Optical Properties. *Science*, *321*(5890), 833-836. doi:10.1126/science.1155296

Andreae, M. O., & Gelencsér, A. (2006). Black carbon or brown carbon? The nature of light-absorbing carbonaceous aerosols. *Atmospheric Chemistry and Physics*, *6*(10), 3131-3148. doi:10.5194/acp-6-3131-2006

Bahadur, R., Praveen, P. S., Xu, Y., & Ramanathan, V. (2012). Solar absorption by elemental and brown carbon determined from spectral observations. *Proceedings of the National Academy of Sciences of the United States of America*, *109*(43), 17366-17371. doi:10.1073/pnas.1205910109

Bonasoni, P., Laj, P., Marinoni, A., Sprenger, M., Angelini, F., Arduini, J., et al. (2010). Atmospheric Brown Clouds in the Himalayas: first two years of continuous observations at the Nepal Climate Observatory-Pyramid (5079 m). *Atmospheric Chemistry and Physics*, *10*(15), 7515-7531. doi:10.5194/acp-10-7515-2010

Bond, T. C., Streets, D. G., Yarber, K. F., Nelson, S. M., Woo, J.-H., & Klimont, Z. (2004). A technology-based global inventory of black and organic carbon emissions from combustion. *Journal of Geophysical Research: Atmospheres, 109*(D14), doi:10.1029/2003JD003697

Boville, B. A., Rasch, P. J., Hack, J. J., & McCaa, J. R. (2006). Representation of Clouds and Precipitation Processes in the Community Atmosphere Model Version 3 (CAM3). *Journal of Climate, 19*(11), 2184-2198. doi:10.1175/JCLI3749.1

Cess, R. D. (1985). Nuclear war: Illustrative effects of atmospheric smoke and dust upon solar radiation. *Climatic Change*, 7(2), 237-251. doi:10.1007/bf00140508

Chen, Y., & Bond, T. C. (2010). Light absorption by organic carbon from wood combustion. *Atmospheric Chemistry and Physics*, *10*(4), 1773-1787. doi:10.5194/acp-10-1773-2010

Chu, J.-E., & Ha, K.-J. (2016). Quantifying organic aerosol single scattering albedo over the tropical biomass burning regions. *Atmospheric Environment*, *147*, 67-78. doi:http://dx.doi.org/10.1016/j.atmosenv.2016.09.069

Chung, C. E., Ramanathan, V., & Decremer, D. (2012). Observationally constrained estimates of carbonaceous aerosol radiative forcing. *Proceedings of the National Academy of Sciences of the United States of America*, *109*(29), 11624-11629. doi:10.1073/pnas.1203707109

515 Collins, W. D., Bitz, C. M., Blackmon, M. L., Bonan, G. B., Bretherton, C. S., Carton, J. A.,
516 et al. (2006). The Community Climate System Model Version 3 (CCSM3). *Journal of*
517 *Climate, 19*(11), 2122-2143. doi:10.1175/JCLI3761.1
518 Cong, Z., Kawamura, K., Kang, S., & Fu, P. (2015). Penetration of biomass-burning
519 emissions from South Asia through the Himalayas: new insights from atmospheric
520 organic acids. *Scientific Reports*, *5*, 9580. doi:10.1038/srep09580
521 Feng, Y., Ramanathan, V., & Kotamarthi, V. R. (2013). Brown carbon: a significant
522 atmospheric absorber of solar radiation? *Atmospheric Chemistry and Physics, 13*(17),
523 8607-8621. doi:10.5194/acp-13-8607-2013
524 Hack, J. J., Caron, J. M., Yeager, S. G., Oleson, K. W., Holland, M. M., Truesdale, J. E., &
525 Rasch, P. J. (2006). Simulation of the Global Hydrological Cycle in the CCSM
526 Community Atmosphere Model Version 3 (CAM3): Mean Features. *Journal of Climate,*
527 *19*(11), 2199-2221. doi:10.1175/JCLI3755.1
528 Heald, C. L., Coe, H., Jimenez, J. L., Weber, R. J., Bahreini, R., Middlebrook, A. M., et al.
529 (2011). Exploring the vertical profile of atmospheric organic aerosol: comparing 17
530 aircraft field campaigns with a global model. *Atmospheric Chemistry and Physics,*
531 *11*(24), 12673-12696. doi:10.5194/acp-11-12673-2011
532 Hess, M., Koepke, P., & Schult, I. (1998). Optical Properties of Aerosols and Clouds: The
533 Software Package OPAC. *Bulletin of the American Meteorological Society*, *79*(5), 831-
534 844. doi:10.1175/1520-0477(1998)079<0831:opoaac>2.0.co;2
535 Huang, Y., Wu, S., Dubey, M. K., & French, N. H. F. (2013). Impact of aging mechanism on
536 model simulated carbonaceous aerosols. *Atmospheric Chemistry and Physics, 13*(13),
537 6329-6343. doi:10.5194/acp-13-6329-2013
538 Ichoku, C., & Ellison, L. (2014). Global top-down smoke-aerosol emissions estimation using
539 satellite fire radiative power measurements. *Atmospheric Chemistry and Physics*, *14*(13),
540 6643-6667. doi:10.5194/acp-14-6643-2014
541 Inness, A., Benedetti, A., Flemming, J., Huijnen, V., Kaiser, J. W., Parrington, M., & Remy,
542 S. (2015). The ENSO signal in atmospheric composition fields: emission-driven versus
543 dynamically induced changes. *Atmospheric Chemistry and Physics, 15*(15), 9083-9097.
544 doi:10.5194/acp-15-9083-2015
545 Kalnay, E., Kanamitsu, M., Kistler, R., Collins, W., Deaven, D., Gandin, L., et al. (1996).
546 The NCEP/NCAR 40-Year Reanalysis Project. *Bulletin of the American Meteorological*
547 *Society*, *77*(3), 437-471. doi:10.1175/1520-0477(1996)077<0437:TNYRP>2.0.CO;2

548 Laskin, A., Laskin, J., & Nizkorodov, S. A. (2015). Chemistry of Atmospheric Brown
549 Carbon. *Chemical Reviews, 115*(10), 4335-4382. doi:10.1021/cr5006167
550 Lau, K. M., & Kim, K. M. (2006). Observational relationships between aerosol and Asian
551 monsoon rainfall, and circulation. *Geophysical Research Letters*, *33*(21).
552 doi:10.1029/2006GL027546
553 Lau, K. M., Kim, M. K., & Kim, K. M. (2006). Asian summer monsoon anomalies induced
554 by aerosol direct forcing: the role of the Tibetan Plateau. *Climate Dynamics*, *26*(7), 855-
555 864. doi:10.1007/s00382-006-0114-z
556 Lau, W. K. M. (2016). The aerosol-monsoon climate system of Asia: A new paradigm.
557 *Journal of Meteorological Research, 30*(1), 1-11. doi:10.1007/s13351-015-5999-1
558 Lau, W. K. M., Kim, K.-M., Shi, J.-J., Matsui, T., Chin, M., Tan, Q., et al. (2017). Impacts of
559 aerosol–monsoon interaction on rainfall and circulation over Northern India and the
560 Himalaya Foothills. *Climate Dynamics, 49*(5), 1945-1960. doi:10.1007/s00382-016-
561 3430-y
562 Lau, W. K. M., Kim, M.-K., Kim, K.-M., & Lee, W.-S. (2010). Enhanced surface warming
563 and accelerated snow melt in the Himalayas and Tibetan Plateau induced by absorbing
564 aerosols. *Environmental Research Letters*, *5*(2), 025204.
565 doi:http://dx.doi.org/10.1088/1748-9326/5/2/025204
566 Lee, K., & Chung, C. E. (2013). Observationally-constrained estimates of global fine-mode
567 AOD. *Atmospheric Chemistry and Physics*, *13*(5), 2907-2921. doi:10.5194/acp-13-
568 2907-2013
569 Liousse, C., Penner, J. E., Chuang, C., Walton, J. J., Eddleman, H., & Cachier, H. (1996). A
570 global three-dimensional model study of carbonaceous aerosols. *Journal of Geophysical*
571 *Research: Atmospheres, 101*(D14), 19411-19432. doi:10.1029/95JD03426
572 Liu, B., Liu, Y., Wu, G., Yan, J., He, J., & Ren, S. (2015). Asian summer monsoon onset
573 barrier and its formation mechanism. *Climate Dynamics*, *45*(3), 711-726.
574 doi:10.1007/s00382-014-2296-0
575 Lou, S., Russell, L. M., Yang, Y., Liu, Y., Singh, B., & Ghan, S. J. (2017). Impacts of
576 interactive dust and its direct radiative forcing on interannual variations of temperature
577 and precipitation in winter over East Asia. *Journal of Geophysical Research:*
578 *Atmospheres, 122*(16), 8761-8780. doi:10.1002/2017JD027267
579 Lou, S., Russell, L. M., Yang, Y., Xu, L., Lamjiri, M. A., DeFlorio, M. J., et al., (2016).
580 Impacts of the East Asian Monsoon on springtime dust concentrations over China.

581 *Journal of Geophysical Research: Atmospheres, 121*(13), 8137-8152.
582 doi:10.1002/2016JD024758
583 Menon, S., Hansen, J., Nazarenko, L., & Luo, Y. (2002). Climate Effects of Black Carbon
584 Aerosols in China and India. *Science*, *297*(5590), 2250-2253.
585 doi:10.1126/science.1075159
586 Moosmüller, H., Chakrabarty, R. K., & Arnott, W. P. (2009). Aerosol light absorption and its
587 measurement: A review. *Journal of Quantitative Spectroscopy and Radiative Transfer*,
588 *110*(11), 844-878. doi:http://dx.doi.org/10.1016/j.jqsrt.2009.02.035
589 Myhre, G. (2009). Consistency Between Satellite-Derived and Modeled Estimates of the
590 Direct Aerosol Effect. *Science*, *325*(5937), 187-190. doi:10.1126/science.1174461
591 Myhre, G., Bellouin, N., Berglen, T. F., Berntsen, T. K., Boucher, O., Grini, A. L. F., et al.
592 (2007). Comparison of the radiative properties and direct radiative effect of aerosols
593 from a global aerosol model and remote sensing data over ocean. *Tellus B: Chemical*
594 *and Physical Meteorology, 59*(1), 115-129. doi:10.1111/j.1600-0889.2006.00226.x
595 Neale, R. B., Richter, J., Park, S., Lauritzen, P. H., Vavrus, S. J., Rasch, P. J., & Zhang, M.
596 (2013). The Mean Climate of the Community Atmosphere Model (CAM4) in Forced
597 SST and Fully Coupled Experiments. *Journal of Climate*, *26*(14), 5150-5168.
598 doi:10.1175/jcli-d-12-00236.1
599 Park, R. J., Kim, M. J., Jeong, J. I., Youn, D., & Kim, S. (2010). A contribution of brown
600 carbon aerosol to the aerosol light absorption and its radiative forcing in East Asia.
601 *Atmospheric Environment*, *44*(11), 1414-1421.
602 doi:http://dx.doi.org/10.1016/j.atmosenv.2010.01.042
603 Qian, Y., Flanner, M. G., Leung, L. R., & Wang, W. (2011). Sensitivity studies on the
604 impacts of Tibetan Plateau snowpack pollution on the Asian hydrological cycle and
605 monsoon climate. *Atmospheric Chemistry and Physics*, *11*(5), 1929-1948.
606 doi:10.5194/acp-11-1929-2011
607 Ramanathan, V., & Carmichael, G. (2008). Global and regional climate changes due to black
608 carbon. *Nature Geoscience*, *1*(4), 221-227. doi:10.1038/ngeo156
609 Rasch, P. J., Mahowald, N. M., & Eaton, B. E. (1997). Representations of transport,
610 convection, and the hydrologic cycle in chemical transport models: Implications for the
611 modeling of short-lived and soluble species. *Journal of Geophysical Research:*
612 *Atmospheres, 102*(D23), 28127-28138. doi:10.1029/97JD02087

613 Roxy, M. K., Ritika, K., Terray, P., Murtugudde, R., Ashok, K., & Goswami, B. N. (2015).
614 Drying of Indian subcontinent by rapid Indian Ocean warming and a weakening land-
615 sea thermal gradient. *Nature Communications, 6*, 7423. doi:10.1038/ncomms8423
616 Stowe, L. L., Ignatov, A. M., & Singh, R. R. (1997). Development, validation, and potential
617 enhancements to the second-generation operational aerosol product at the National
618 Environmental Satellite, Data, and Information Service of the National Oceanic and
619 Atmospheric Administration. *Journal of Geophysical Research: Atmospheres,*
620 *102*(D14), 16923-16934. doi:10.1029/96JD02132
621 Takemura, T., Egashira, M., Matsuzawa, K., Ichijo, H., O'Ishi, R., & Abe-Ouchi, A. (2009).
622 A simulation of the global distribution and radiative forcing of soil dust aerosols at the
623 Last Glacial Maximum. *Atmospheric Chemistry and Physics*, *9*(9), 3061-3073.
624 doi:10.5194/acp-9-3061-2009
625 Takemura, T., Nozawa, T., Emori, S., Nakajima, T. Y., & Nakajima, T. (2005). Simulation of
626 climate response to aerosol direct and indirect effects with aerosol transport-radiation
627 model. *Journal of Geophysical Research: Atmospheres*, *110*(D2).
628 doi:10.1029/2004JD005029
629 Vinoj, V., Rasch, P. J., Wang, H., Yoon, J.-H., Ma, P.-L., Landu, K., & Singh, B. (2014).
630 Short-term modulation of Indian summer monsoon rainfall by West Asian dust. *Nature*
631 *Geoscience*, *7*(4), 308-313. doi:10.1038/ngeo2107
632 Wang, C. (2007). Impact of direct radiative forcing of black carbon aerosols on tropical
633 convective precipitation. *Geophysical Research Letters*, *34*(5).
634 doi:10.1029/2006GL028416
635 Yang, Y., Russell, L. M., Lou, S., Liao, H., Guo, J., Liu, Y., et al. (2017). Dust-wind
636 interactions can intensify aerosol pollution over eastern China. *Nature Communications,*
637 *8*, 15333. doi:10.1038/ncomms15333
638 Zender, C. S., Bian, H., & Newman, D. (2003). Mineral Dust Entrainment and Deposition
639 (DEAD) model: Description and 1990s dust climatology. *Journal of Geophysical*
640 *Research: Atmospheres*, *108*(D14). doi:10.1029/2002JD002775
641 Zhang, H., Wang, Z., Guo, P., & Wang, Z. (2009). A modeling study of the effects of direct
642 radiative forcing due to carbonaceous aerosol on the climate in East Asia. *Advances in*
643 *Atmospheric Sciences*, *26*(1), 57-66. doi:10.1007/s00376-009-0057-5
644

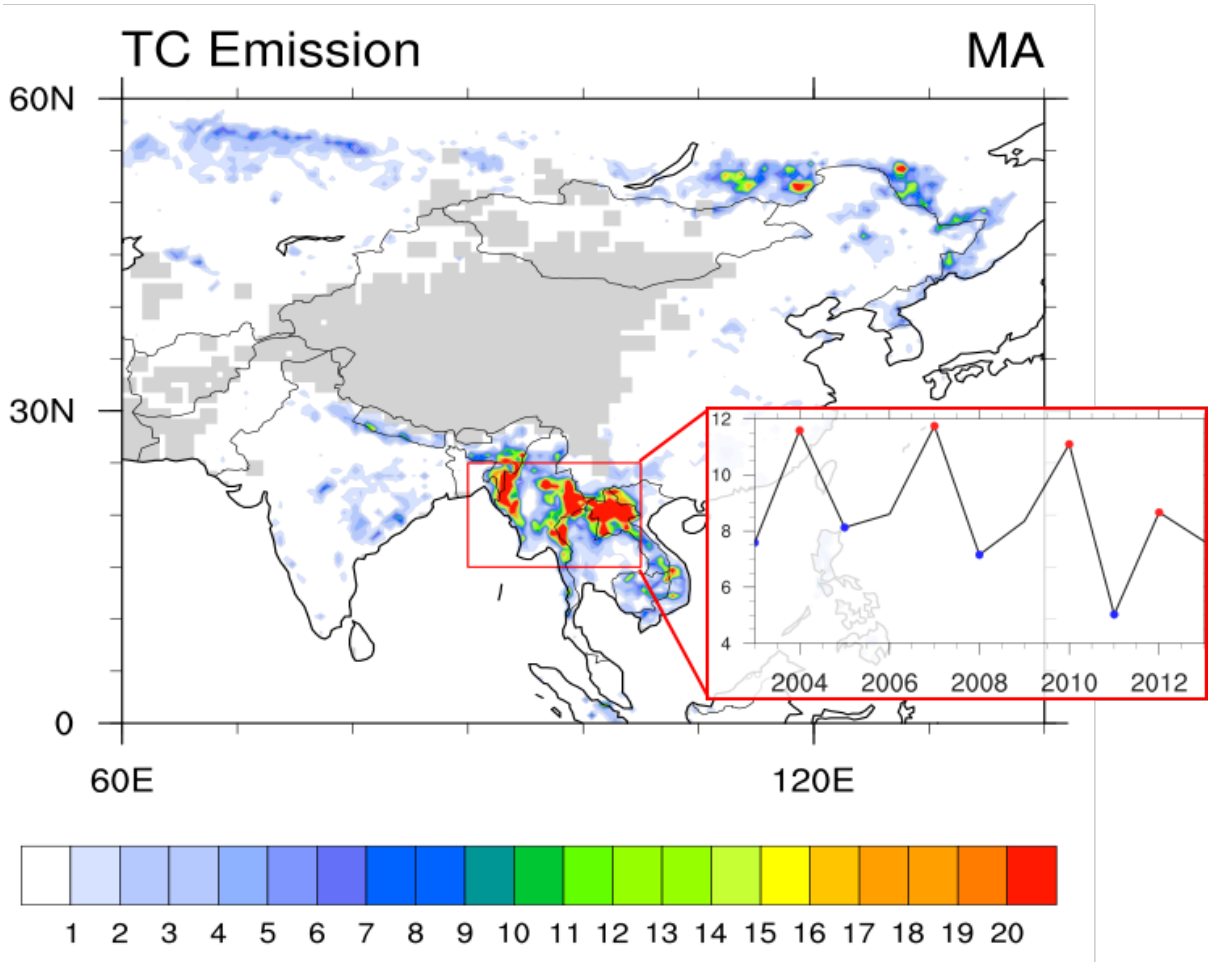

Figure 1. Springtime biomass burning emission over Asian region. Fire Energetics and Emissions Research (FEER) v.1 emission estimates of total carbon (TC) based on MODIS 2003–2013 Fire Radiative Power and AOT observations from Terra and Aqua over the Asian region, averaged for March to April on a 0.5° x 0.5°-resolution global grid. The time series in the red box is March to April averaged TC emissions over Southeast Asia (15°N-25°N, 90°E-105°E).

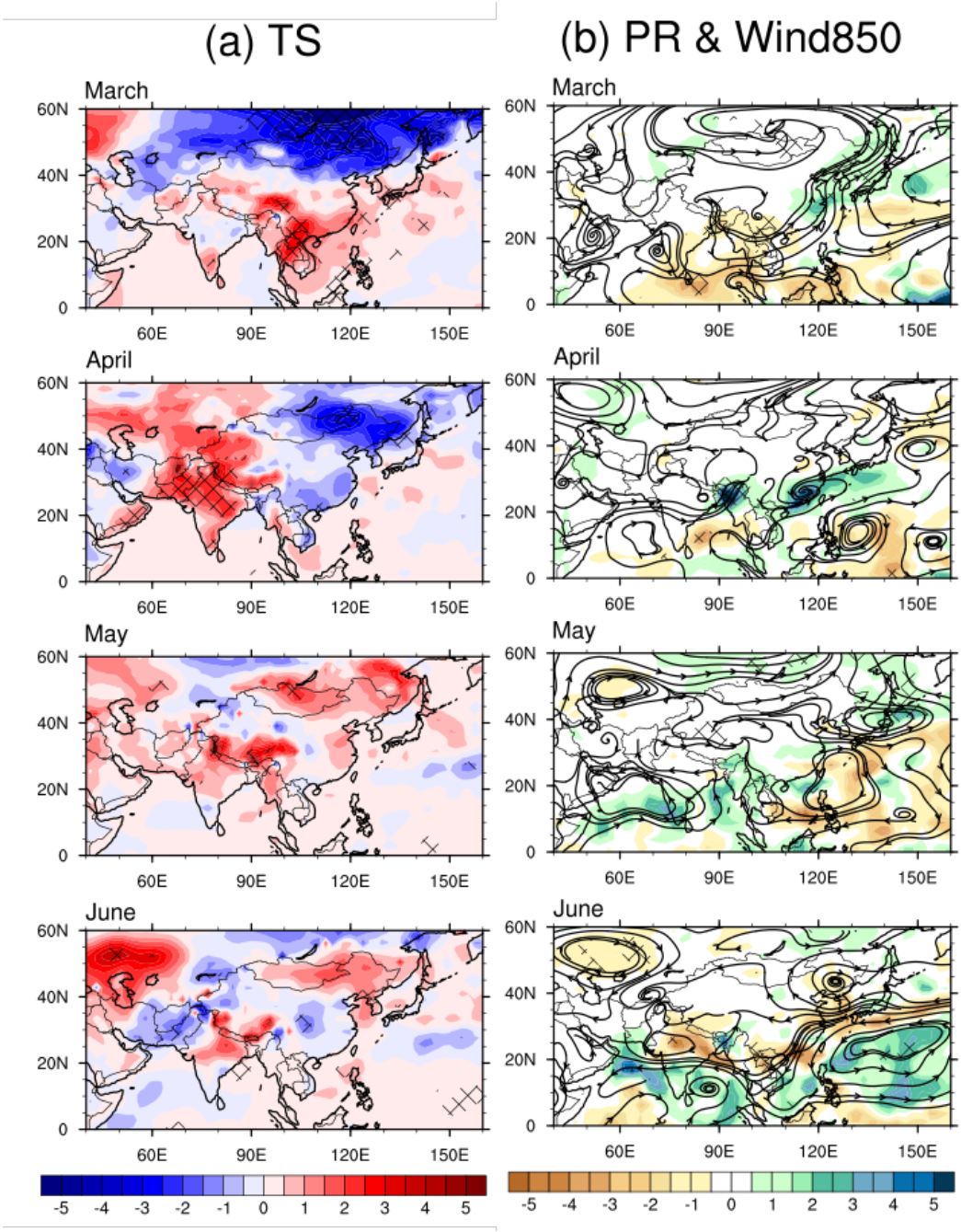

Figure 2. Observed composite differences between strong and weak TC emission years. (a) Surface temperature and (b) precipitation and streamlines at 850 hPa from March to June. The strong and weak emission years were selected based on the accumulated TC emission from March to April over Southeast Asia (15°N–25°N, 90°E–105°E; Figure 1). The selected high- and low-emission years are 2004, 2007, 2010, and 2012 and 2003, 2005, 2008, and 2011, respectively. The crosshatched areas indicate a statistical significance of the Student's t-test at the 90% level.

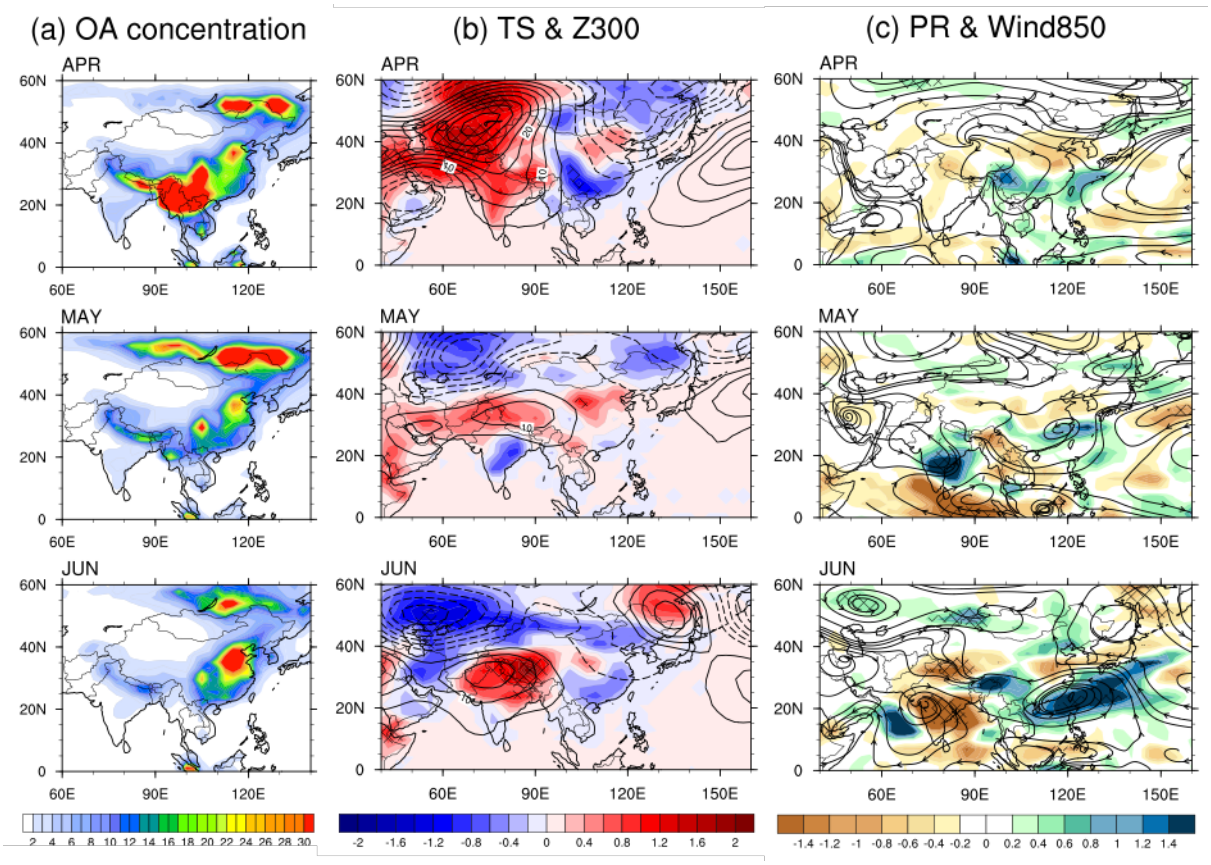

662

663 **Figure 3.** Prescribed OA concentration and changes in Asian monsoon climate due to
664 enhanced OA light absorption obtained from CAM4 experiments. The left panel (a) indicates
665 the vertically integrated organic carbon concentration (10^{-6} g/kg) prescribed in CAM4, the
666 middle panel (b) represents changes in surface temperature (shading) and geopotential height
667 at 300 hPa, and right panel is for (c) precipitation (shading) and 850 hPa (vector) streamlines
668 for April (upper), May (middle), and June (lower). The crosshatched areas indicate statistical
669 significance of the Student's t-test at the 90% level. The organic carbon is the sum of the
670 hydrophobic and hydrophilic organic carbon.

671

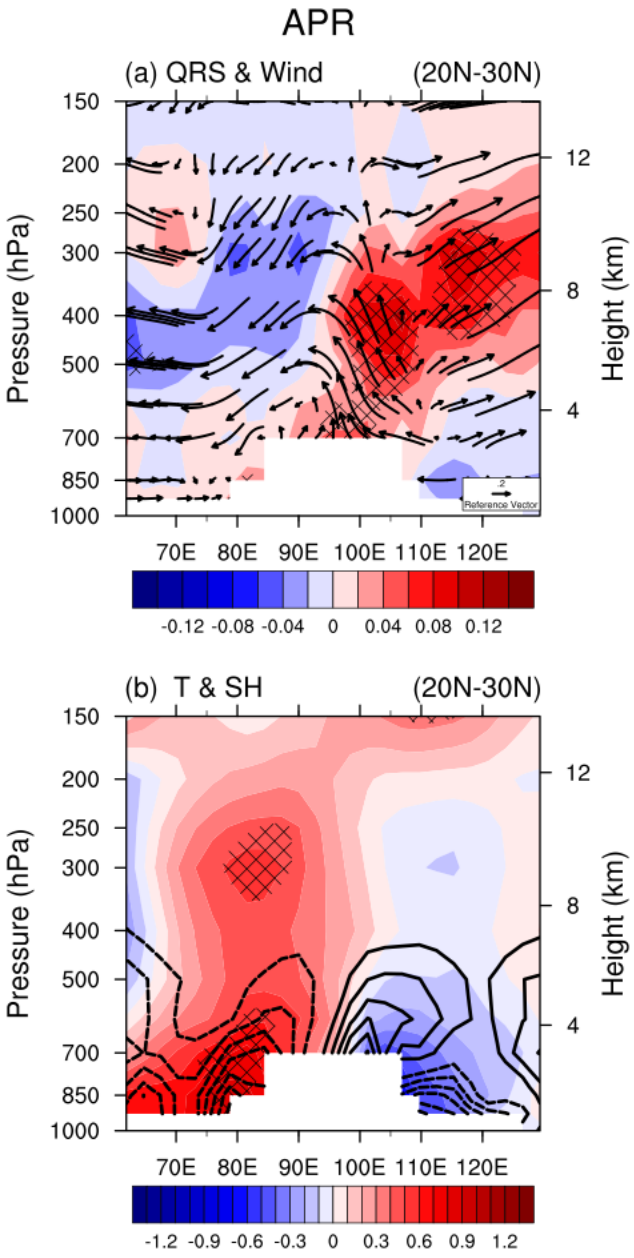

672

673 **Figure 4.** Longitude-height cross section of the atmospheric response to OA heating over
674 southeast Asian region in April. (a) Solar heating rate (QRS, shading) and wind anomalies
675 (vector) and (b) air temperature (T, shading) and specific humidity (SH, contour). The graphs
676 are latitudinally averaged over 20°N–30°N to examine upward motion around the source
677 region. The unit of the vertical velocity (specific humidity) is $2*10^{-2}$ ms^{-1} (0.05 g/kg). The
678 positive (negative) values for SH are plotted as solid (dashed) lines.

679

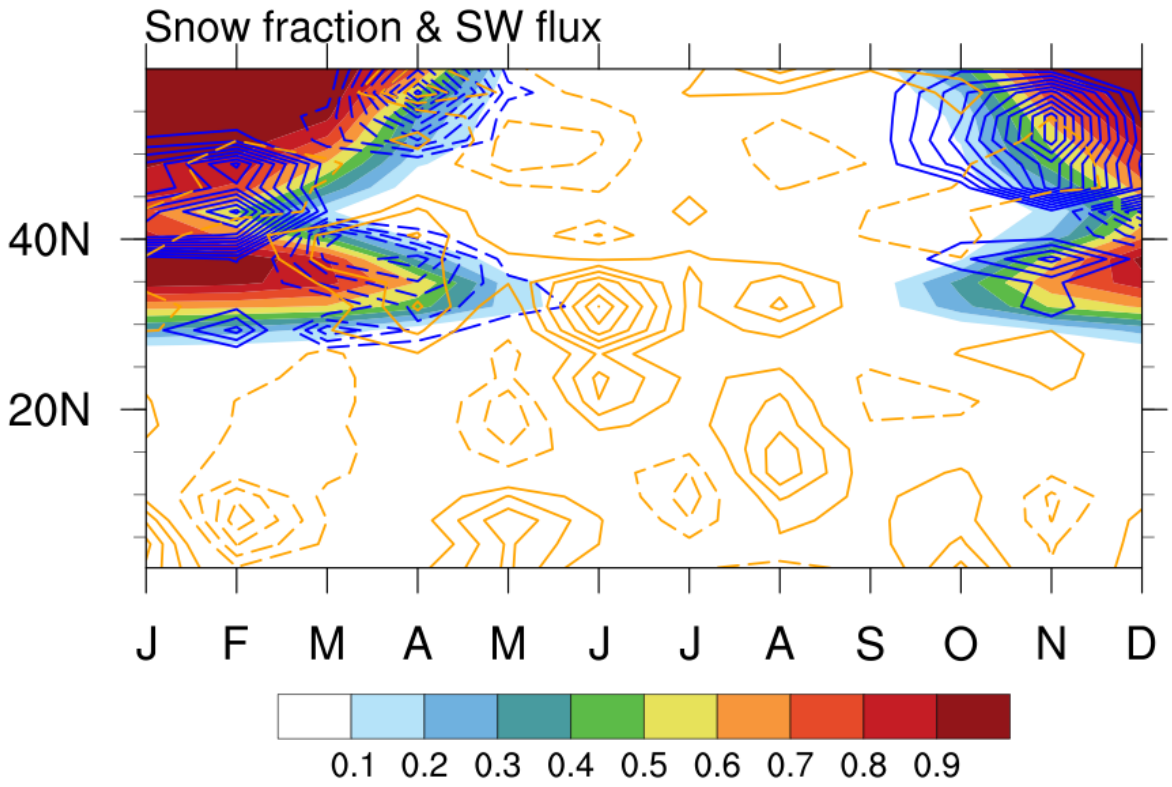

680

681 **Figure 5.** Monthly Snow fraction and shortwave flux associated with enhanced OA light
682 absorption. The shading indicates mean snow fraction in EXP_SCA experiment and blue and
683 orange contours represent changes in snow fraction and shortwave flux (i.e., EXP_ABS
684 minus EXP_SCA). The graphs are longitudinally averaged over 70°E-90°E to examined OA
685 impact on snow melting over Tibetan Plateau. The unit of the fluxes are Wm^{-2}. Contour
686 interval for snow fraction is 0.01 and that for shortwave is 3 Wm^{-2}. The positive (negative)
687 values are plotted as solid (dashed) lines.

688

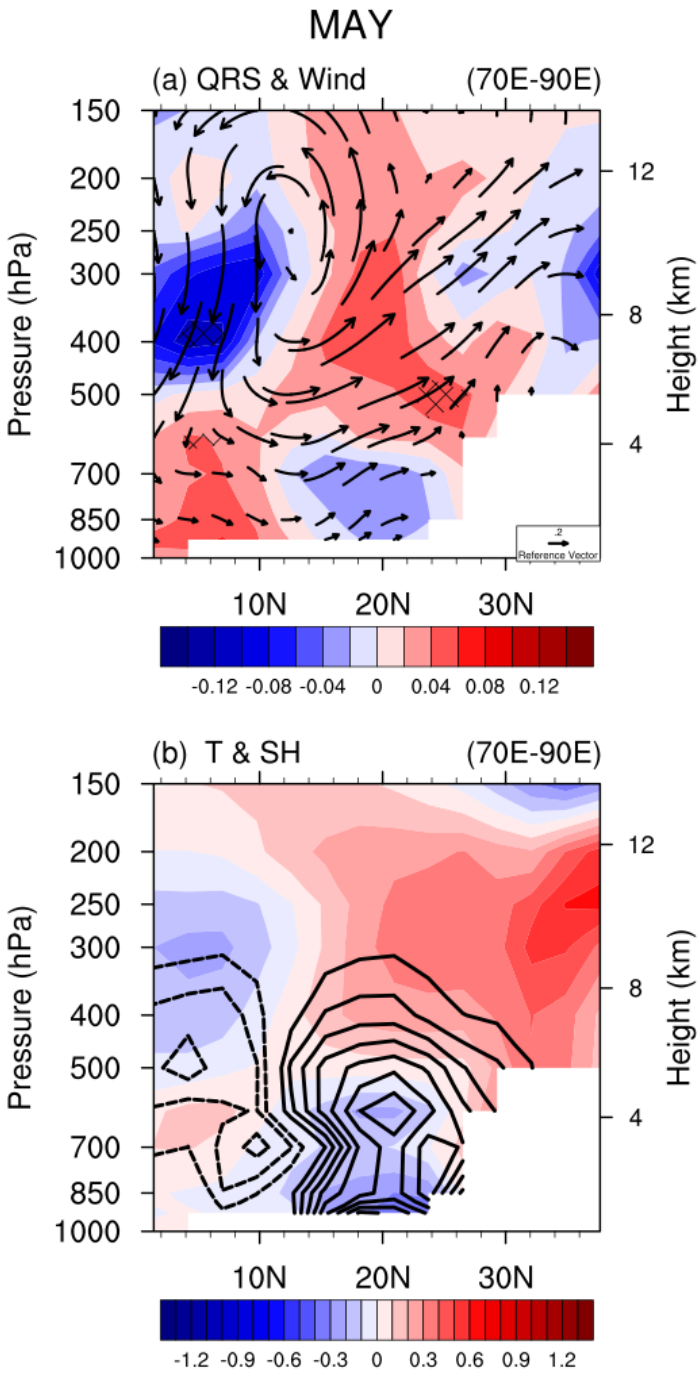

689

690 **Figure 6.** Latitude-height cross section averaged over 70°E–90°E in May. (a) QRS (shading)
691 and wind anomalies (vector) and (b) T (shading) and SH (contour). The graphs are
692 longitudinally averaged over 70°E–90°E to examine enhanced meridional overturning
693 circulation and strengthening of Indian summer monsoon.

694

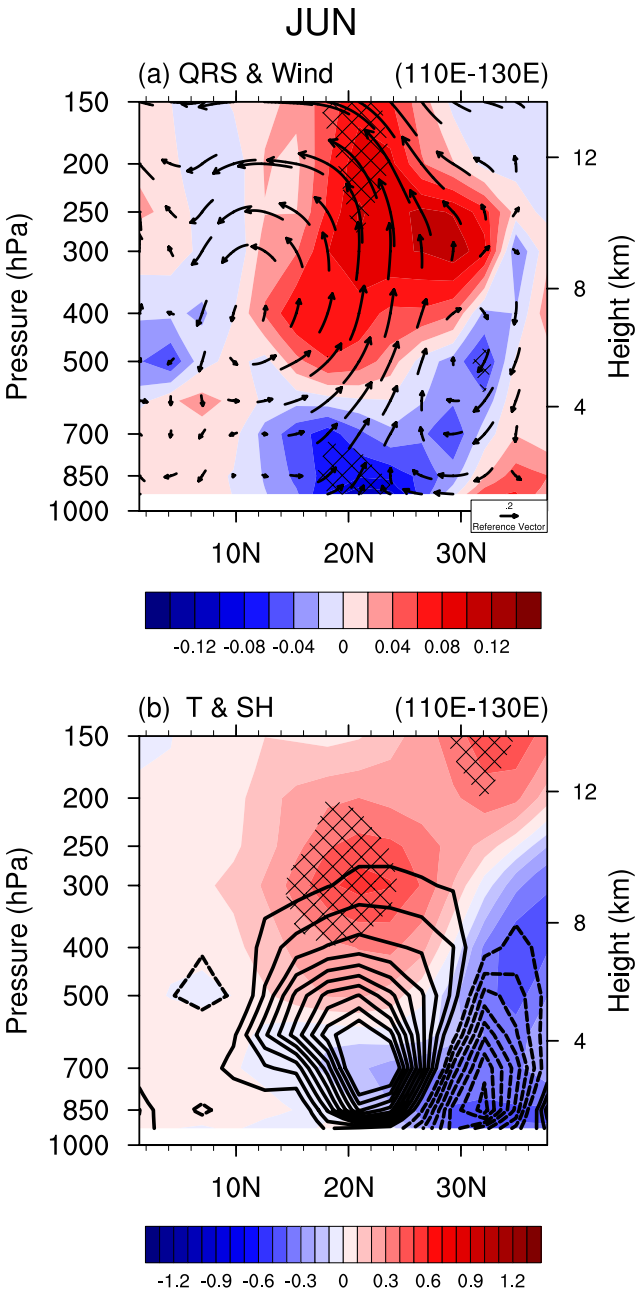

695

696 **Figure 7.** Same as in Figure 6 but averaged over 110°E–130°E in June.

697

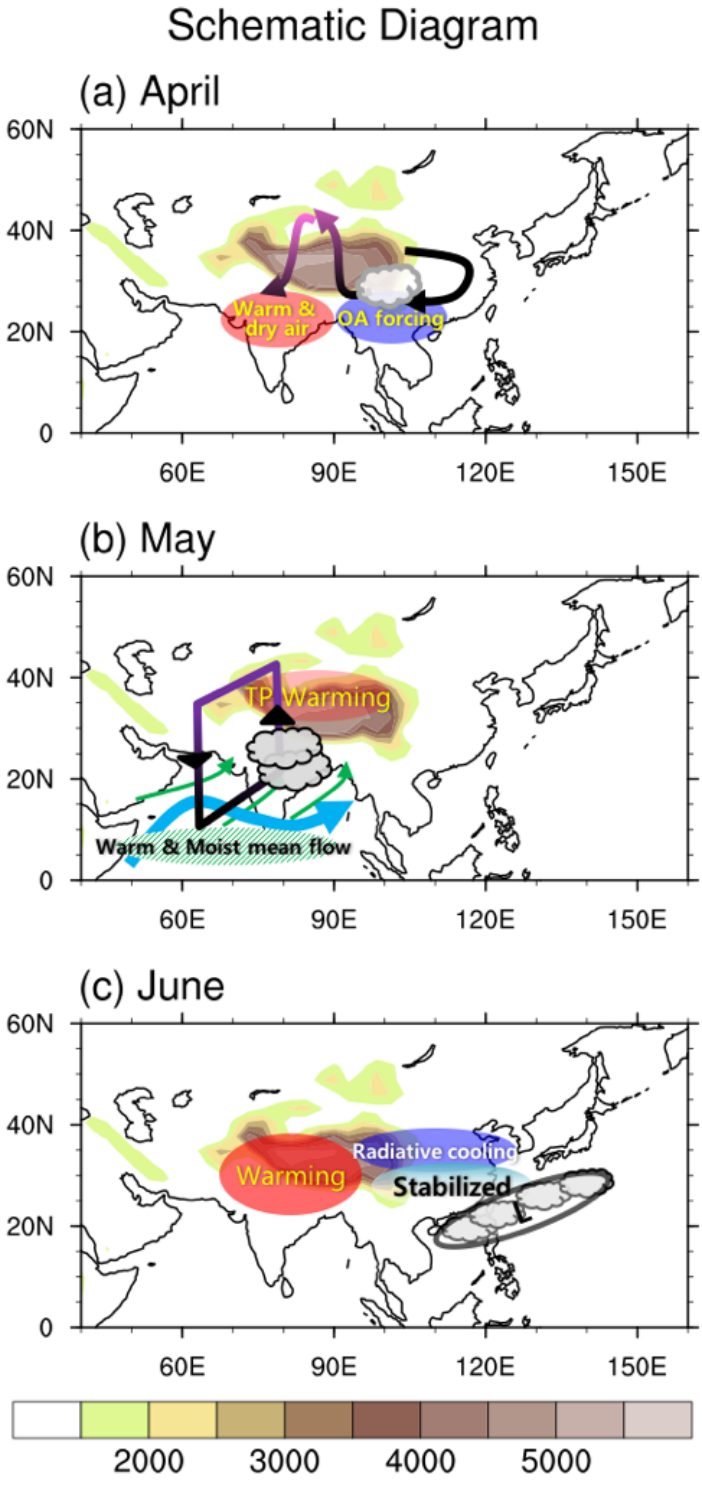

698

699 **Figure 8.** Schematic diagram of OA light absorption effect. Figure summarizes the
700 mechanisms of how the OA light absorption influences Asian summer monsoon from April
701 to June.